This is an open access article published under an ACS AuthorChoice License, which permits copying and redistribution of the article or any adaptations for non-commercial purposes.

THE JOURNAL OF PHYSICAL CHEMISTRY B

Article

pubs.acs.org/JPCB

Chemical Shielding Anisotropies for Chloroform Exchanging between a Free Site and a Complex with Cryptophane-D: A Cross-Correlated NMR Relaxation Study

Emilie Steiner,[†] Thierry Brotin,[‡] Zoltan Takacs,[†] and Jozef Kowalewski*[,†]

[†]Department of Materials and Environmental Chemistry, Arrhenius Laboratory, Stockholm University, SE-106 91 Stockholm, Sweden

[‡]Laboratoire de Chimie, (CNRS-UMR 5182) Ecole Normale Supérieure de Lyon, 46 Allée d'Italie, F-69364 Lyon cedex 07, France

Supporting Information

ABSTRACT: The case of ^{13}C-labeled chloroform exchanging between a free site in solution and the encaged site within the cryptophane-D cavity is investigated using the measurements of longitudinal cross-correlated relaxation rates, involving the interference of the dipole−dipole and chemical shielding anisotropy interactions. A compact theoretical expression is provided, along with an experimental protocol, based on INEPT (insensitive nuclei enhanced by polarization)-enhanced double-quantum-filtered inversion recovery measurements. The analysis of the build-up curves results in a set of cross-correlated relaxation rates for both the ^{13}C and ^{1}H spins at the two sites. It is demonstrated that the results can be given a consistent interpretation in terms of molecular-level properties, such as rotational correlation times, the Lipari−Szabo order parameter, and interaction strength constants. The analysis yields the bound-site carbon-13 chemical shielding anisotropy, $\Delta\sigma_C = -58 \pm 8$ ppm, in good agreement with most recent liquid-crystal measurements and the corresponding proton shielding anisotropy, $\Delta\sigma_H = 14 \pm 2$ ppm.

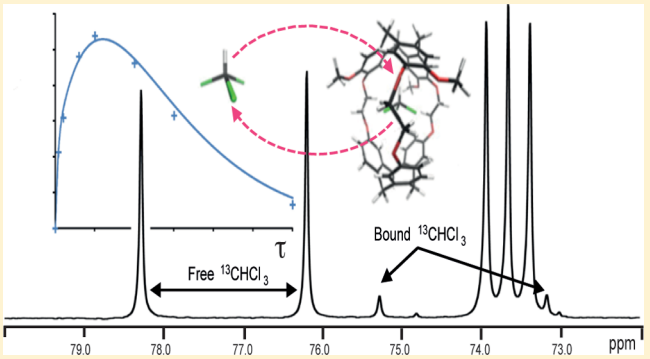

1. INTRODUCTION

Cryptophanes are cagelike molecules composed of two rather rigid cyclotribenzylene caps connected by three linkers whose length and nature can be varied. These host molecules can bind in solution small molecular guests (such as chloromethanes) within their cavity. The first cryptophane—cryptophane-A with three identical ethylenedioxy linkers and each of the phenyl rings carrying one methoxy substituent—was synthesized and characterized by Collet and co-workers in the early eighties.[1−3] The chemistry and the physical properties of these systems were reviewed some time ago.[4] These molecules are still of great interest in today's chemistry, and in recent years, studies of cryptophane complexes have moved in different directions. For instance, a lot of attention was directed toward the preparation of enantiopure compounds and the study of their chiroptical properties.[5−11] Another promising direction of research was concerned with complexes of xenon and their use as sensors or magnetic resonance imaging probes.[12−22] Yet other types of monatomic species of interest were monovalent cations and their interactions with water-soluble cryptophanes.[7,23,24] One of the most interesting properties of cryptophane derivatives lies in their ability to reversibly encapsulate and to isolate a unique guest molecule. Interestingly, the guest molecule trapped within the cavity can have very different properties than the one dissolved in the bulk. Therefore, this feature makes cryptophanes of great interest for scientists studying the physical behavior of the isolated guest molecule trapped in the cavity of a host. Recently, a series of papers have dealt with investigations of dynamic processes in solutions of cryptophane complexes of chloromethanes[25−30] and other small molecules,[31] using NMR spectroscopy. Finally, we wish to mention some work on crystalline cryptophane systems, studied by X-ray diffraction and/or solid-state NMR.[25,30,32,33]

This article is in a way a continuation of the extensive NMR investigation of cryptophane-D (Scheme 1) inclusion complexes with dichloromethane and chloroform in solution,[27] reported in

Scheme 1. Cryptophane-D

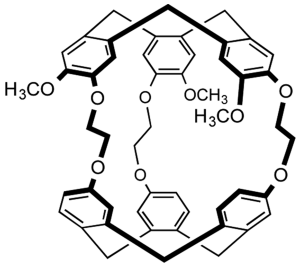

Received: June 1, 2015
Revised: August 12, 2015
Published: August 12, 2015

© 2015 American Chemical Society

DOI: 10.1021/acs.jpcb.5b05218
J. Phys. Chem. B 2015, 119, 11760−11767

2012. The case of chloroform as a guest offers interesting possibilities for relaxation work since the chemical exchange between the free and bound sites is slow on the chemical shift time scale and not too fast to blur the spin relaxation properties of the two sites.[34] Thus, we presented in that work the ^{13}C spin−lattice relaxation rate (obtained under broadband decoupling of protons) and heteronuclear NOE (nuclear Overhauser enhancement) measurements at one temperature (280 K) and three magnetic fields. The analysis of the results confirmed that the free site was in the extreme narrowing range[35] while the bound site was not. The bound site results were interpreted in terms the Lipari−Szabo model.[36] In this article, we wish to extend the study of spin relaxation in this system to the $^{13}C-^{1}H$ system in free and bound chloroform, making use of experiments allowing the cross-correlated relaxation (CCR) phenomena to come into play. After taking into consideration chemical exchange, this allows us to follow the changes in the anisotropies of ^{13}C and ^{1}H chemical shielding tensors for chloroform caused by cryptophane complex formation.

The concept of cross-correlated relaxation—or relaxation interference—refers to phenomena involving more than one spin interaction.[35,37,38] The interactions at hand need to have the same tensorial rank. For a system of two spin $^{1}/_{2}$ nuclei, the most common CCR phenomenon is the interference of the dipole−dipole (DD) interaction and the chemical shielding anisotropy (CSA), both rank two interactions.[39,40] In larger systems of spin $^{1}/_{2}$ species, the interference of different dipolar interactions can also occur.[41,42] Here, we are interested in the interplay of the CCR phenomena and chemical exchange.

This interplay can, by and large, take three forms. (1) Difference between double-quantum and zero-quantum relaxation rates in two-spin systems. Kloiber and Konrat[43] and Früh et al.[44] showed that the cross-correlated modulation of isotropic chemical shifts of the two spins (e.g., amide ^{15}N and ^{1}H in proteins) by chemical exchange gives rise to the differential rate, while Lundström and Akke reported a careful analysis of the contributing mechanisms.[45] (2) Combination of the conventional measurements of the spin−spin relaxation rate (R_2) or the relaxation rate in the rotating frame ($R_{1\rho}$) and the DD-CSA CCR rate applied to separate the exchange and nonexchange contributions to the conventional rates.[46−48] (3) Exchange effects in longitudinal relaxation. The case when one of the spins in a multispin system undergoes intermolecular chemical exchange was discussed by Skrynnikov and Ernst[49] and more recently by Esadze et al.[50] and Werbeck and Hansen.[51] Here, we investigate the case when the whole two-spin system exchanges between two sites. The issue is closely related to the exchange phenomena in the *zz* spectroscopy introduced a long time ago by Bodenhausen, Wagner, and co-workers.[52,53]

The outline of this article is as follows. Section 2 describes the theoretical background, and section 3 presents the experiments details. The results are presented and discussed in section 4, and the conclusions are drawn in section 5.

2. THEORY

The longitudinal relaxation processes in the two-spin *IS* system can be described by a relaxation matrix:[35,40,54,55]

$$\frac{\mathrm{d}}{\mathrm{d}t}\begin{pmatrix}\langle I_z\rangle\\ \langle S_z\rangle\\ \langle 2I_zS_z\rangle\end{pmatrix} = -\begin{pmatrix}\Gamma_{11} & \Gamma_{12} & \Gamma_{13}\\ \Gamma_{21} & \Gamma_{22} & \Gamma_{23}\\ \Gamma_{31} & \Gamma_{32} & \Gamma_{33}\end{pmatrix}\begin{pmatrix}\langle I_z\rangle - I_z^{\mathrm{eq}}\\ \langle S_z\rangle - S_z^{\mathrm{eq}}\\ \langle 2I_zS_z\rangle\end{pmatrix} \tag{1}$$

The symbols $\langle I_z\rangle$, $\langle S_z\rangle$, and $\langle 2I_zS_z\rangle$ denote the expectation values of the corresponding operators, while I_z^{eq} and S_z^{eq} represent the equilibrium magnetizations. The symmetric relaxation matrix with elements Γ_{ij} contains various rate constants. The diagonal elements Γ_{11} and Γ_{22} correspond to spin−lattice relaxation rates, R_1, for the *I* spin (here ^{1}H) and the *S* spin (^{13}C), respectively. Γ_{33} is the decay rate for the longitudinal two-spin order, $\langle 2I_zS_z\rangle$, $\Gamma_{12} = \Gamma_{21}$ is the cross-relaxation rate, σ_{CH}, and the remaining terms are the DD-CSA CCR rates. The relaxation matrix elements are, according to Redfield theory,[35,56] expressed in terms of spectral densities, $J(\omega)$, taken at various frequencies corresponding to energy differences in the spin system. Using the normalization convention of Kowalewski and Mäler,[35] the following expressions apply:

$$\Gamma_{11} = \frac{\pi}{5}b_{CH}{}^{2}[J_{CH,CH}(\omega_H - \omega_C) + 3J_{CH,CH}(\omega_H) + 6J_{CH,CH}(\omega_H + \omega_C)] + \frac{4\pi}{15}c_H{}^{2}J_{H,H}(\omega_H) \tag{2a}$$

$$\Gamma_{22} = \frac{\pi}{5}b_{CH}{}^{2}[J_{CH,CH}(\omega_H - \omega_C) + 3J_{CH,CH}(\omega_C) + 6J_{CH,CH}(\omega_H + \omega_C)] + \frac{4\pi}{15}c_C{}^{2}J_{C,C}(\omega_C) \tag{2b}$$

$$\Gamma_{12} = \frac{\pi}{5}b_{CH}{}^{2}[6J_{CH,CH}(\omega_H + \omega_C) - J_{CH,CH}(\omega_H - \omega_C)] \tag{2c}$$

$$\Gamma_{13} = \Gamma_{31} = \delta_{H,CH} = \frac{4\pi}{5}b_{CH}c_HJ_{CH,H}(\omega_I) \tag{2d}$$

$$\Gamma_{23} = \Gamma_{32} = \delta_{C,CH} = \frac{4\pi}{5}b_{CH}c_CJ_{CH,C}(\omega_C) \tag{2e}$$

$$\Gamma_{33} = \frac{3\pi}{5}b_{CH}{}^{2}J_{CH,CH}(\omega_C) + \frac{3\pi}{5}b_{CH}{}^{2}J_{CH,CH}(\omega_H) + \frac{4\pi}{15}c^{2}{}_{H}J_{H,H}(\omega_H) + \frac{4\pi}{15}c^{2}{}_{C}J_{C,C}(\omega_C) \tag{2f}$$

where b_{CH} denotes the dipole−dipole coupling constant,

$$b_{CH} = -\frac{\mu_0\gamma_I\gamma_S\hbar}{4\pi r_{IS}{}^{3}} \tag{3}$$

with all of the symbols having their usual meaning, with $c_H = \gamma_H B_0\Delta\sigma(H)$ and $\Delta\sigma(H)$ being the proton (*I*-spin) chemical shielding anisotropy. c_C and $\Delta\sigma(C)$ are the corresponding quantities for carbon-13 (*S* spin). We return to the definitions of spectral densities below. In principle, the scalar relaxation of the second kind,[35,57] originating in *J* couplings to the quadrupolar chlorine isotopes (^{35}Cl, ^{37}Cl), may be operative but can safely be neglected for spin−lattice relaxation. For the free-site relaxation, the spin rotation interaction[35] may also be considered, but we neglect it too.

When chemical exchange between two sites, free (f) and bound (b), is present, the relaxation in the spin system is formulated in terms of a direct sum[58] of the expressions similar to eq 1 but allowing for separate operators and block-diagonal matrix segments for the two sites, as well as including the free-to-bound (k_{fb}) and bound-to-free (k_{bf}) first-order rate constants coupling the two blocks:

DOI: 10.1021/acs.jpcb.5b05218
J. Phys. Chem. B 2015, 119, 11760−11767

$$\frac{\mathrm{d}}{\mathrm{d}t}\begin{pmatrix}\langle I_z\rangle_\mathrm{f}\\ \langle S_z\rangle_\mathrm{f}\\ \langle 2I_zS_z\rangle_\mathrm{f}\\ \langle I_z\rangle_\mathrm{b}\\ \langle S_z\rangle_\mathrm{b}\\ \langle 2I_zS_z\rangle_\mathrm{b}\end{pmatrix} = -\begin{pmatrix}\Gamma^\mathrm{f}_{11}+k_\mathrm{fb} & \Gamma^\mathrm{f}_{12} & \Gamma^\mathrm{f}_{13} & -k_\mathrm{bf} & 0 & 0\\ \Gamma^\mathrm{f}_{21} & \Gamma^\mathrm{f}_{22}+k_\mathrm{fb} & \Gamma^\mathrm{f}_{23} & 0 & -k_\mathrm{bf} & 0\\ \Gamma^\mathrm{f}_{31} & \Gamma^\mathrm{f}_{32} & \Gamma^\mathrm{f}_{33}+k_\mathrm{fb} & 0 & 0 & -k_\mathrm{bf}\\ -k_\mathrm{fb} & 0 & 0 & \Gamma^\mathrm{b}_{11}+k_\mathrm{bf} & \Gamma^\mathrm{b}_{12} & \Gamma^\mathrm{b}_{13}\\ 0 & -k_\mathrm{fb} & 0 & \Gamma^\mathrm{b}_{21} & \Gamma^\mathrm{b}_{22}+k_\mathrm{bf} & \Gamma^\mathrm{b}_{23}\\ 0 & 0 & -k_\mathrm{fb} & \Gamma^\mathrm{b}_{31} & \Gamma^\mathrm{b}_{32} & \Gamma^\mathrm{b}_{33}+k_\mathrm{bf}\end{pmatrix}\begin{pmatrix}\langle I_z\rangle_\mathrm{f}-I^\mathrm{eq}_{z,\mathrm{f}}\\ \langle S_z\rangle_\mathrm{f}-S^\mathrm{eq}_{z,\mathrm{f}}\\ \langle 2I_zS_z\rangle_\mathrm{f}\\ \langle I_z\rangle_\mathrm{b}-I^\mathrm{eq}_{z,\mathrm{b}}\\ \langle S_z\rangle_\mathrm{b}-S^\mathrm{eq}_{z,\mathrm{b}}\\ \langle 2I_zS_z\rangle_\mathrm{b}\end{pmatrix} \tag{4}$$

The expression in eq 4 is derived by assuming that the exchange processes swap the spins between the two environments but have no effect on the type of spin order. Helgstrand et al.[59] described how to obtain an expression for the time evolution of the full density operator in a coupled two-spin system in the product operator basis, allowing for relaxation and exchange in the context of simulating NMR pulse sequences. Their relaxation and exchange matrix had the dimensionality 30 × 30. The expression in eq 4 is a submatrix of their general case, concerned with the subspace of longitudinal operators. The expression is analogous to the case discussed recently by Auer and coworkers.[60] The transverse relaxation counterpart to eq 4 has been discussed by Peng[48] in the context of ligand−receptor interaction.

The relaxation matrix elements in eq 4 are given by expressions shown in eqs 2a−2f but with interaction strengths and spectral densities characteristic of each site. For the bound site, we use the Lipari−Szabo type[36] spectral density

$$J_\mathrm{b}(\omega) = \frac{1}{2\pi}\left[\frac{S^2\tau_\mathrm{R}}{1+\omega^2{\tau_\mathrm{R}}^2} + (1-S^2)\tau_\mathrm{eff}\right] \tag{5}$$

with ${\tau_\mathrm{eff}}^{-1} = {\tau_\mathrm{R}}^{-1} + {\tau_\mathrm{loc}}^{-1}$ where τ_R is the rank-two correlation time for the isotropic reorientation of the molecule (here, the host−guest system) as a whole and τ_loc is the corresponding correlation time for the local motion (here, of the guest inside the host cavity). It is assumed that the local motion is within the extreme narrowing range. The symbol S^2 is called the generalized order parameter squared, a measure of the restriction of the local motion. The free site (extreme narrowing) spectral density takes on a very simple frequency-independent form

$$J_\mathrm{f}(\omega) = \frac{1}{2\pi}\tau_\mathrm{f} \tag{6}$$

where τ_f is the reorientational correlation time for the free site.

3. EXPERIMENTAL DETAILS

The $CHCl_3$@cryptophane-D solution was the same as sample 4 used in our earlier study,[27] with 46 mM ^{13}C-labeled chloroform and 11 mM cryptophane-D in 1,1,2,2-tetrachloroethane-d_2. NMR experiments were conducted at 280 K on a Bruker Avance III spectrometer operating at 9.4 T using 5 mm BBI and BBO probeheads. The temperature calibration was achieved with a standard methanol calibration sample. ^{1}H and ^{13}C relaxation experiments were performed on free and bound chloroform. A hard $\pi/2$ pulse of 8.9 μs and a $\pi/2$ pulse of 65.6 μs for GARP (globally optimized alternating phase rectangular pulse) decoupling were used for the proton-detected experiments while a hard $\pi/2$ pulse of 7.2 μs and a $\pi/2$ pulse length of 86.5 μs for the broad-band composite pulse decoupling scheme denoted WALTZ-16 were applied in the case of carbon detection.

The longitudinal relaxation times T_1 were measured by inversion recovery with power-gated decoupling (different decoupler power levels were applied during different sections of the pulse sequence). Both ^{1}H and ^{13}C experiments were performed using recovery delays ranging from 0.001 to 70 s and a relaxation delay of 60 s. The number of scans for the proton or carbon-13 experiment was set to 64 or 256, respectively.

In order to quantify the ^{13}C cross-correlated relaxation rates, $\delta_\mathrm{C,CH}$, the buildup of the longitudinal two-spin order magnetization was measured by using the pulse scheme presented in Figure 1. The sequence is based on a heteronuclear double-quantum filtered inversion recovery proposed a long time ago by Jaccard et al.[54] and used in a context similar to ours by Bhattacharyya and Kumar.[61] It is similar to the sequence proposed by Ernst and Ernst[62] for measuring the relaxation interference between two heteronuclear dipolar interactions. By analogy to that work, the sensitivity of the experiment is enhanced by adding an INEPT block at the beginning of the sequence. After the double-quantum filter, the antiphase magnetization of the two-spin order is converted into an in-phase doublet by a $({}^1/_4J_\mathrm{CH} - (\pi)_\mathrm{C,H} - {}^1/_4J_\mathrm{CH})$ spin echo, with J_CH

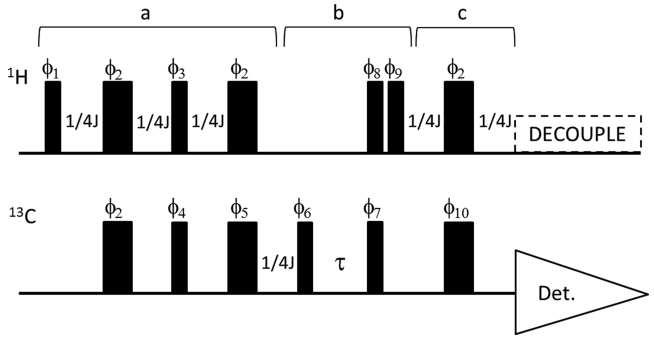

Figure 1. Pulse scheme used for the buildup of the longitudinal two-spin order from ^{13}C polarization. (a) A refocused INEPT block is placed at the beginning to ensure a polarization transfer from proton to carbon. (b) The double-quantum filtered inversion recovery starts and converts the enhanced two-spin order into antiphase magnetization. (c) Antiphase magnetization evolves during a spin echo with respect to $^1J_\mathrm{CH}$ and is converted into in-phase ^{13}C magnetization so that proton decoupling can be applied. The phases of the ϕ pulses are $\phi_1 = (x)_{16}$, $(-x)_{16}$; $\phi_2 = (x)$, $(-x)$; $\phi_3 = (y)_4$, $(-y)_4$; $\phi_4 = (x)_8$, $(y)_8$, $(-x)_8$, $(-y)_8$; $\phi_5 = (x, -x)_4$, $(y, -y)_4$; $\phi_6 = (y, -y)_4$, $(x, -x)_4$; $\phi_7 = (y)_8$, $(x)_8$; $\phi_8 = (x)_8$, $(y)_8$; $\phi_9 = (x, x, -x, -x)_2$, $(y, y, -y, -y)_2$; $\phi_{10} = [(x, -x)_4, (y, -y)_4]_2$, $[(y, -y)_4, (-x, x)_4]_2$, $[(-x, x)_4, (-y, y)_4]_2$, $[(-y, y)_4, (x, -x)_4]_2$; Acq = $[(y, -y, -y, y, y, -y), (-x, x, x, -x, x, -x, -x, x)]_2$, $[(-y, y, y, -y, y, -y, -y, y), (x, -x, -x, x, -x, x, x, -x)]_2$.

DOI: 10.1021/acs.jpcb.5b05218
J. Phys. Chem. B 2015, 119, 11760−11767

equal to 210 Hz in $^{13}CHCl_3$. Proton decoupling is then applied, leading again to an improved signal-to-noise ratio.[35] In order to measure the pure longitudinal two-spin order, the elimination of artifacts (whose effect can be important when measuring weak-magnitude signals) was achieved by a phase cycling adapted first from the refocused INEPT sequence proposed by Bruker. To avoid phase distortion, the four-step phase cycle denoted EXORCYCLE was also applied on the last spin−echo pulse (ϕ10), resulting in 128 phase-cycling steps. In the proton case, ^{1}H cross-correlated relaxation rates were determined from a conventional double-quantum filtered inversion recovery. Build-ups of longitudinal two-spin order (from both proton and carbon-13 longitudinal magnetization) were obtained with recovery delays τ ranging from 0.01 to 60 s. Experiments were performed with 256 scans to achieve a desired signal-to-noise ratio and with a relaxation delay of 100 s to allow the return to equilibrium of carbon and proton magnetizations, both in the free and bound sites.

4. RESULTS AND DISCUSSION

The chloroform and solvent region of the proton-coupled carbon-13 spectrum of our $CHCl_3$@cryptophane-D solution is shown in Figure 2. We can immediately make two important

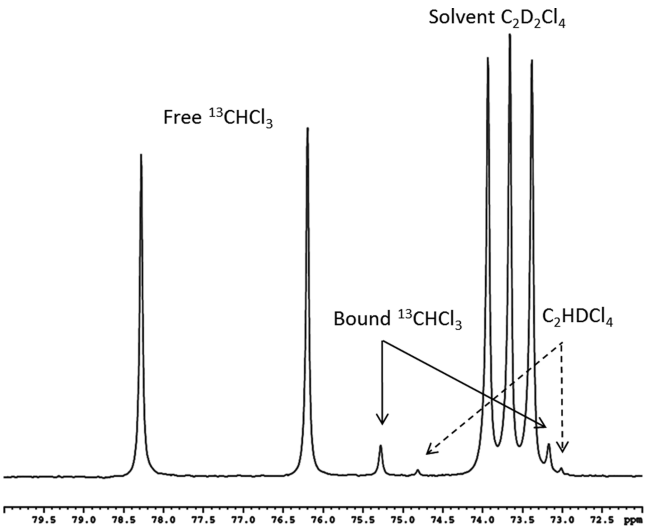

Figure 2. Fragment of proton-coupled carbon-13 spectrum of $^{13}CHCl_3$@cryptophane-D in 1,1,2,2-tetrachloroethane-d_2 recorded at 280 K and 9.4 T.

observations. First, one can readily see that the doublet components corresponding to chloroform in the free site are of unequal intensity. The origin of this phenomenon is the differential line broadening (DLB), the transverse analogue of the longitudinal CCR with the same origin in the DD-CSA interference. For the bound site, the signal intensities are lower and the DLB is not apparent. The second observation is related to the positions of the bound-site doublet with respect to the strong deuterated solvent signal. At 9.4 T, the two components are located on both sides of the solvent triplet. A simple calculation immediately shows that at higher (but still intermediate) magnetic fields, the upfield $^{13}CHCl_3$ line will overlap with the solvent signals. This may be a complication if the measurements described here are performed at higher magnetic fields. We notice also that the ^{13}C complexation shift of about 3 ppm in Figure 2 is in good agreement with the results of proton-decoupled measurements.[27] The corresponding ^{1}H complexation shift was earlier reported as 4.3 ppm, and the association equilibrium constant at 280 K was given as 12.1 M^{-1}.[27]

Next, we move to the data from the double-quantum filtered build-up experiments for ^{13}C and ^{1}H, shown in Figure 3. The build-ups for the free and bound sites are displayed separately because they occur on very different time scales, as all of the spin relaxation processes are much slower in the low-molecular-weight free site than in the medium-sized host−guest complex. Before describing the results of the fitting of the data shown in Figure 3 in terms of different relaxation rate constants, let us quickly go through the parameters which we decided to keep fixed in that process, collected in Table 1. The carbon-13 spin−lattice relaxation rates for both sites ($\Gamma_{22} = R_1(C)$, obtained under proton decoupling) and the exchange rates were taken from our earlier study.[27] The cross-relaxation rate, $\Gamma_{12} = \sigma_{CH}$, for the free site (which is in the extreme narrowing regime) was obtained as $R_1(C)/2$. The proton spin−lattice relaxation rates, $R_1(H)$, were obtained in this work by inversion−recovery measurements with carbon-13 decoupling. The proton R_1 for the free site is slightly larger than the corresponding carbon relaxation rate. For the bound site, the opposite is true, which is likely to be caused by the frequency dependence of the involved spectral densities or perhaps different CSA contributions.

Having fixed the parameters in Table 1, we are left with seven parameters to be fitted to the four build-up curves. Experimental build-ups corresponding to the free and the bound sites are fitted simultaneously by using the whole relaxation matrix, describing the relaxation of the coupled *IS* spin system (eq 4). The relaxation matrices for the two sites are constructed by introducing the fixed parameters from Table 1 and by choosing estimated starting values for the remaining unknowns: the CCR rates, Γ_{33} for both sites, and σ^b_{CH}. The evolution of the two-spin orders $\langle 2I_zS_z\rangle_f$ and $\langle 2I_zS_z\rangle_b$ is determined by numerically solving the system of differential equations. Depending on the double-quantum filtered build-up experiment performed (carbon or proton), initial and equilibrium conditions for the I, S, and $2I_zS_z$ magnetizations are defined as in Table 2. A nonlinear least-squares fitting procedure, making use of the Matlab Simplex routine,[63] is then applied for parameter optimization. The fitting of the build-up data in Figure 3 results in the rates summarized in Table 3. Their corresponding errors are obtained from 500 Monte Carlo iterations by assuming a 5% error in the experimental data.

The CCR rates, $\Gamma^f_{13} = \Gamma^f_{31}$ and $\Gamma^f_{23} = \Gamma^f_{32}$, and the two-spin order decay rate, Γ^f_{33}, are indeed all very small compared to the corresponding quantities for the bound site. The next step in the analysis is to interpret the rates in Tables 1 and 3 in terms of molecular parameters describing the interaction strengths and reorientational dynamics and to make use of possible redundancies. For the free chloroform, the carbon-13 spin−lattice relaxation rate can immediately be translated into an effective correlation time,[35] τ^{eff}_c (free), if we know the CH interatomic distance or the $^{13}C^1H$ dipole−dipole coupling constant. Assuming r_{CH} = 109.8 pm[64] yields τ^{eff}_c (free) = 4.4 ps, a reasonable value for a small molecule in a low-viscosity solvent. Alternatively, we might use r_{CH} = 107.3 pm, based on the microwave studies of chloroform.[65] Depending on the choice of r_{CH}, the other molecular properties will have slightly different values. The results are summarized in Table 4.

The dynamic parameters (correlation times, S^2) for the bound chloroform in the former case (the third column) were taken from Takacs et al.[27] and were based on R_1 and heteronuclear

DOI: 10.1021/acs.jpcb.5b05218
J. Phys. Chem. B 2015, 119, 11760−11767

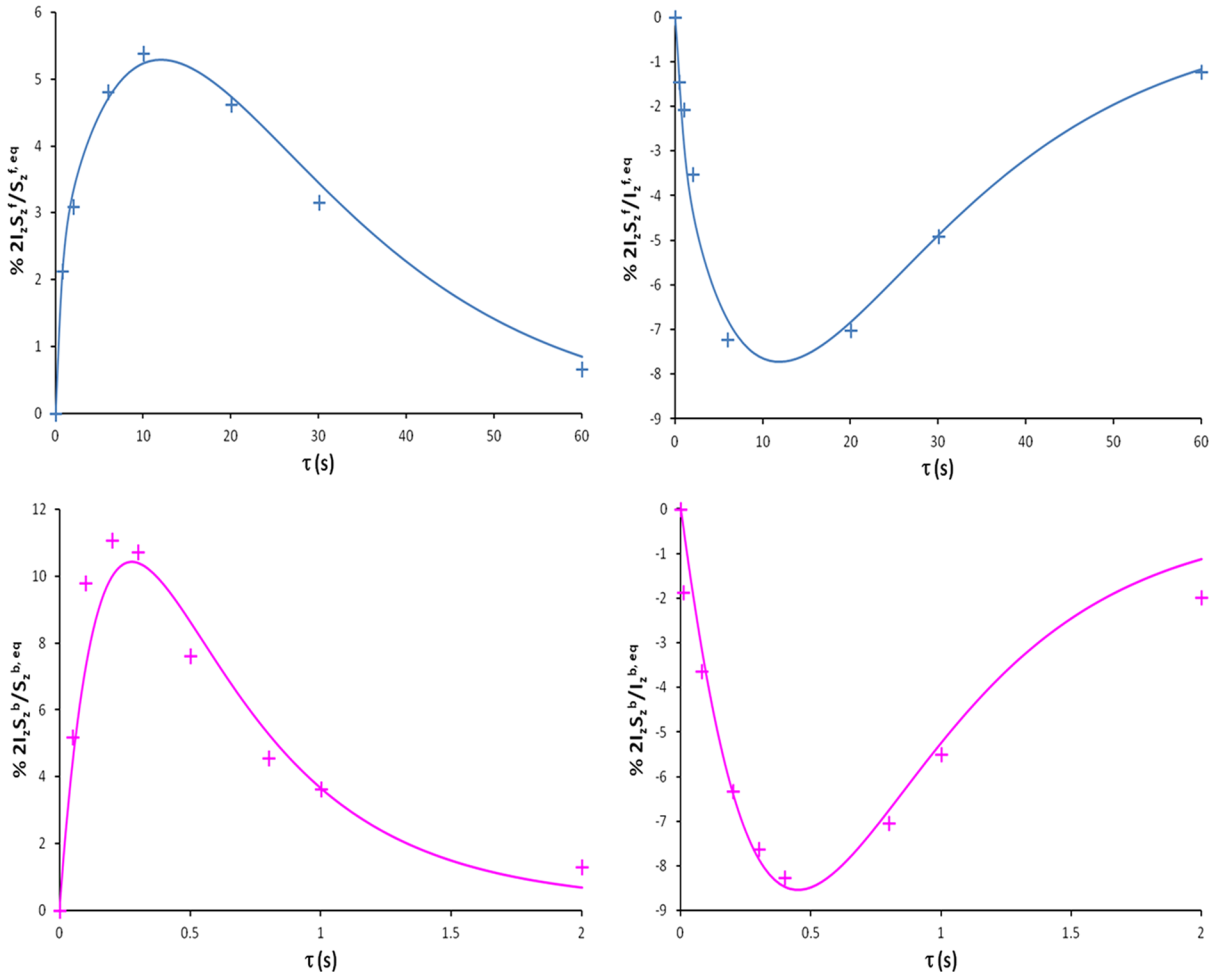

Figure 3. Build-ups of the longitudinal two-spin order from ^{13}C (two left panels) and proton (two right panels) polarizations for free (two top panels) and bound (two bottom panels) sites. The vertical axes show expectation values of $2I_zS_z$ normalized to the refocused INEPT intensities in the case of ^{13}C data and to the intensities after recording a single-pulse NMR spectrum in the case of ^{1}H.

Table 1. Parameters Kept Constant in the Fitting of the Build-Up Curves

parameter	value
R_1^f (C), s^{-1}	0.09
R_1^f (H), s^{-1}	0.11
σ_{CH}^f, s^{-1}	0.045
R_1^b (C), s^{-1}	3.6
R_1^b (H), s^{-1}	2.8
k_{fb}, s^{-1}	0.02
k_{bf}, s^{-1}	0.25

Table 2. Initial and Equilibrium Conditions for the I, S, and $2I_zS_z$ Magnetizations Used for Solving the System of Differential Equations (eq 4)

	initial conditions			equilibrium conditions		
	I	S	$2I_zS_z$	I	S	$2I_zS_z$
^{13}C build-up experiment	$I_{z,f}^{eq}$	$-I_{z,f}^{eq}$	0	$I_{z,f}^{eq}$	$(\gamma_C/\gamma_H)I_{z,f}^{eq}$	0
^{1}H build-up experiment	$-I_{z,f}^{eq}$	$S_{z,f}^{eq}$	0	$I_{z,f}^{eq}$	$S_{z,f}^{eq}$	0

NOE data at three magnetic fields. We notice that S^2 is about 0.5−0.6, which indicates a limited reorientational freedom for the guest inside the host cavity. The corresponding data for the shorter CH distance were obtained by fitting the same three

Table 3. Parameters Adjusted by Fitting to the Build-Up Data in Figure 2

parameter	value
$\delta_{C,CH}^f$, s^{-1}	0.0053 ± 0.0004
$\delta_{H,CH}^f$, s^{-1}	−0.0058 ± 0.0004
Γ_{33}^f, s^{-1}	0.050 ± 0.004
$\delta_{C,CH}^b$, s^{-1}	0.85 ± 0.07
$\delta_{H,CH}^b$, s^{-1}	−0.22 ± 0.02
Γ_{33}^b, s^{-1}	4.0 ± 1.0
σ_{CH}^b, s^{-1}	1.2 ± 0.1

fields data to the Lipari−Szabo model with a modified dipolar coupling constant. The chemical shielding parameters are determined by the CCR rates (the CSA contributions to the spin−lattice relaxation rates are negligible), so the relative errors are expected to be the same as for these quantities (Table 3). The differences between the $\Delta\sigma$ values corresponding to the two values of the carbon−proton distance are not very large. The free chloroform anisotropies are in reasonable agreement with the values reported a long time ago for chloroform dissolved in ethylene glycol by Mäler and Kowalewski[66] ($\Delta\sigma(C) = -32 \pm 8$ ppm, $\Delta\sigma(H) = 12 \pm 2$ ppm from CCR rates in isotropic solution) and by Bhattacharyya and Dailey[67] ($\Delta\sigma(C) = -39 \pm 1$ ppm, $\Delta\sigma(H) = 9.8 \pm 2.5$ ppm, based on a liquid-crystalline (LC) solution). Higher absolute values of $\Delta\sigma(C)$ values for chloro-

DOI: 10.1021/acs.jpcb.5b05218
J. Phys. Chem. B 2015, 119, 11760−11767

Table 4. Molecular Quantities Derived from the Relaxation Rates in Tables 3 and 1

property	assumed r_{CH} = 107.3 pm	assumed r_{CH} = 109.8 pm
τ_f, ps	3.8 ± 0.1	4.4 ± 0.1
τ_R, ps	830 ± 81[a]	830 ± 81[a]
S^2	0.52 ± 0.04	0.60 ± 0.04[a]
τ_{loc}, ps	25 ± 7	34 ± 9[a]
$\Delta\sigma^f$ (C), ppm	−36 ± 3	−33 ± 3
$\Delta\sigma^f$ (H), ppm	8.0 ± 1.0	7.4 ± 0.9
$\Delta\sigma^b$ (C), ppm	−62 ± 9	−58 ± 8
$\Delta\sigma^b$ (H), ppm	15 ± 2	14 ± 2

[a]The value was taken from Takacs et al.[27] on the basis of the relaxation of the cryptophane host.

form were reported in more recent work on LC systems.[68−70] The latter two papers also presented somewhat scattered $\Delta\sigma$(H) values as well as results of quantum chemical calculations.

The values for the host−guest complex are more interesting. Clearly, both shielding anisotropies in Table 4 increase significantly as a consequence of encaging. Marjanska et al.[71] were the first to deal with the changes in carbon CSAs upon trapping chloroform inside a cryptophane, again using the LC methodology. The difference between the $\Delta\sigma$(C) values reported in that study was rather small. In a more recent communication from the same group, Chaffee and co-workers[72] reported $\Delta\sigma(C) = -37 \pm 9$ ppm for free chloroform in an LC solution, while $\Delta\sigma(C) = -54 \pm 15$ ppm was given for a chloroform molecule trapped inside the cryptophane-A cavity in the same LC system. Our present results for carbon CSA agree very well with these values.

The next issue we want to discuss is concerned with redundancies in the data sets presented in Tables 1 and 3 if the results of dynamic models in Table 4 are taken into consideration. For example, Γ_{33} values can be computed using eq 2f and the interaction strengths/dynamic parameters of Table 4. Thus, calculated values of the two-spin order decay rates are 0.055 s^{-1} for the free site and 5.1 s^{-1} for the encaged site, in decent agreement with the data in Table 3. Another relaxation rate that can be given a theoretical (or back-calculated) value is the bound-site cross-relaxation rate. Here, the agreement between the value in Table 3 and the back-calculated 0.62 s^{-1} is much less satisfactory. As an alternative to this analysis, we have also performed a global fit of the build-ups directly optimizing the molecular parameters, making use of eqs 2a−2f, 3, 5, and 6. The results are presented in the Supporting Information. Altogether, we believe that our analysis demonstrates that the multiparameter analysis of the complex relaxation and exchange network can be performed in a reliable way.

5. CONCLUDING REMARKS

We have in this article provided a theoretical expression for the longitudinal relaxation in a heteronuclear two-spin system in the presence of a two-site exchange process transferring the whole two-spin system between two sites. We also propose an experimental protocol, based on INEPT-enhanced measurements of double-quantum filtered inversion recovery-type experiments. We apply the theory and the experimental protocol for the case of ^{13}C-labeled chloroform exchanging between a free site in solution and the encaged site within the cryptophane-D cavity. Numerical fitting of the build-up curves results in a set of CCR rates for both the ^{13}C and ^{1}H spins at the two sites. It is demonstrated that the results can be given a consistent interpretation in terms of molecular-level properties, such as rotational correlation times, the Lipari−Szabo order parameter, and interaction strength constants. As a highlight of the study, we stress that we found it possible to evaluate the CSA for both ^{1}H and ^{13}C in the bound site. In the case of the carbon-13 chemical shielding anisotropies, the present analysis is in good agreement with most recent liquid-crystal measurements.

■ ASSOCIATED CONTENT

Supporting Information

The Supporting Information is available free of charge on the ACS Publications website at DOI: 10.1021/acs.jpcb.5b05218.

Full references for papers with more than 10 authors. One additional table. (PDF)

■ AUTHOR INFORMATION

Corresponding Author

*E-mail: jozef.kowalewski@mmk.su.se.

Present Address

(E.S.) Department of Medical Biochemistry and Biophysics (MBB), Scheeles Väg 2, Karolinska Institute, SE.171 77 Stockholm, Sweden.

Notes

The authors declare no competing financial interest.

■ ACKNOWLEDGMENTS

This work was supported by the Swedish Research Council (grant no. 613-2011-3311) and the Carl Tryggers Foundation. We thank Mr. Torbjörn Astlind for his help with the NMR spectrometer.

■ REFERENCES

(1) Collet, A.; Gottarelli, G. Circular-Dichroism and Absolute-Configuration of C3-Chiral Derivatives of Cyclotriveratrylene. *J. Am. Chem. Soc.* **1981**, *103*, 204−205.

(2) Gabard, J.; Collet, A. Synthesis of A (D3)-Bis(Cyclotriveratrylenyl) Macrocage by Stereospecific Replication of A (C3)-Subunit. *J. Chem. Soc., Chem. Commun.* **1981**, 1137−1139.

(3) Collet, A.; Gabard, J.; Jacques, J.; Cesario, M.; Guilhem, J.; Pascard, C. Synthesis and Absolute-Configuration of Chiral (C-3) Cyclotriveratrylene Derivatives - Crystal-Structure of (M)-(−)-2,7,12-Triethoxy-3,8,13-Tris-[(R)-1-Methoxycarbonylethoxy]-10,15 -Dihydro-5H-Tribenzo[A,D,G]-Cyclononene. *J. Chem. Soc., Perkin Trans. 1* **1981**, 1630−1638.

(4) Brotin, T.; Dutasta, J. P. Cryptophanes and Their Complexes-Present and Future. *Chem. Rev.* **2009**, *109*, 88−130.

(5) Brotin, T.; Vanthuyne, N.; Cavagnat, D.; Ducasse, L.; Buffeteau, T. Chiroptical Properties of Nona- and Dodecamethoxy Cryptophanes. *J. Org. Chem.* **2014**, *79*, 6028−6036.

(6) Daugey, N.; Brotin, T.; Vanthuyne, N.; Cavagnat, D.; Buffeteau, T. Raman Optical Activity of Enantiopure Cryptophanes. *J. Phys. Chem. B* **2014**, *118*, 5211−5217.

(7) Brotin, T.; Guy, L.; Martinez, A.; Dutasta, J. P. Enantiopure Supramolecular Cages: Synthesis and Chiral Recognition Properties. *Differentiation of Enantiomers II*; Topics in Current Chemistry; Springer: Berlin, 2013; Vol. 341, pp 177−230.

(8) Bouchet, A.; Brotin, T.; Linares, M.; Cavagnat, D.; Buffeteau, T. Influence of the Chemical Structure of Water-Soluble Cryptophanes on Their Overall Chiroptical and Binding Properties. *J. Org. Chem.* **2011**, *76*, 7816−7825.

(9) Bouchet, A.; Brotin, T.; Linares, M.; Ågren, H.; Cavagnat, D.; Buffeteau, T. Enantioselective Complexation of Chiral Propylene Oxide by an Enantiopure Water-Soluble Cryptophane. *J. Org. Chem.* **2011**, *76*, 4178−4181.

DOI: 10.1021/acs.jpcb.5b05218
J. Phys. Chem. B 2015, 119, 11760−11767

(10) Bouchet, A.; Brotin, T.; Linares, M.; Ågren, H.; Cavagnat, D.; Buffeteau, T. Conformational Effects Induced by Guest Encapsulation in an Enantiopure Water-Soluble Cryptophane. *J. Org. Chem.* **2011**, *76*, 1372−1383.
(11) Bouchet, A.; Brotin, T.; Cavagnat, D.; Buffeteau, T. Induced Chiroptical Changes of a Water-Soluble Cryptophane by Encapsulation of Guest Molecules and Counterion Effects. *Chem. - Eur. J.* **2010**, *16*, 4507−4518.
(12) Schröder, L.; Lowery, T. J.; Hilty, C.; Wemmer, D. E.; Pines, A. Molecular Imaging Using a Targeted Magnetic Resonance Hyperpolarized Biosensor. *Science* **2006**, *314*, 446−449.
(13) Rose, H. M.; Witte, C.; Rossella, F.; Klippel, S.; Freund, C.; Schröder, L. Development of an Antibody-Based, Modular Biosensor for Xe-129 NMR Molecular Imaging of Cells at Nanomolar Concentrations. *Proc. Natl. Acad. Sci. U. S. A.* **2014**, *111*, 11697−11702.
(14) Klippel, S.; Döpfert, J.; Jayapaul, J.; Kunth, M.; Rossella, F.; Schnurr, M.; Witte, C.; Freund, C.; Schröder, L. Cell Tracking with Caged Xenon: Using Cryptophanes as MRI Reporters upon Cellular Internalization. *Angew. Chem., Int. Ed.* **2014**, *53*, 493−496.
(15) Spence, M. M.; Rubin, S. M.; Dimitrov, I. E.; Ruiz, E. J.; Wemmer, D. E.; Pines, A.; Yao, S. Q.; Tian, F.; Schultz, P. G. Functionalized Xenon as a Biosensor. *Proc. Natl. Acad. Sci. U. S. A.* **2001**, *98*, 10654−10657.
(16) Aaron, J. A.; Chambers, J. M.; Jude, K. M.; Di Costanzo, L.; Dmochowski, I. J.; Christianson, D. W. Structure of a (129)Xe-Cryptophane Biosensor Complexed with Human Carbonic Anhydrase II. *J. Am. Chem. Soc.* **2008**, *130*, 6942−6943.
(17) Tassali, N.; Kotera, N.; Boutin, C.; Leonce, E.; Boulard, Y.; Rousseau, B.; Dubost, E.; Taran, F.; Brotin, T.; Dutasta, J. P.; et al. Smart Detection of Toxic Metal Ions, Pb^{2+} and Cd^{2+}, Using a Xe-129 NMR-Based Sensor. *Anal. Chem.* **2014**, *86*, 1783−1788.
(18) Boutin, C.; Leonce, E.; Brotin, T.; Jerschow, A.; Berthault, P. Ultrafast Z-Spectroscopy for Xe-129 NMR-Based Sensors. *J. Phys. Chem. Lett.* **2013**, *4*, 4172−4176.
(19) Kotera, N.; Tassali, N.; Leonce, E.; Boutin, C.; Berthault, P.; Brotin, T.; Dutasta, J. P.; Delacour, L.; Traore, T.; Buisson, D. A.; et al. A Sensitive Zinc-Activated ^{129}Xe MRI Probe. *Angew. Chem., Int. Ed.* **2012**, *51*, 4100−4103.
(20) Boutin, C.; Stopin, A.; Lenda, F.; Brotin, T.; Dutasta, J. P.; Jamin, N.; Sanson, A.; Boulard, Y.; Leteurtre, F.; Huber, G.; et al. Cell Uptake of a Biosensor Detected by Hyperpolarized Xe-129 NMR: The Transferrin Case. *Bioorg. Med. Chem.* **2011**, *19*, 4135−4143.
(21) Fairchild, R. M.; Joseph, A. I.; Holman, K. T.; Fogarty, H. A.; Brotin, T.; Dutasta, J. P.; Boutin, C.; Huber, G.; Berthault, P. A Water-Soluble Xe@cryptophane-111 Complex Exhibits Very High Thermodynamic Stability and a Peculiar Xe-129 NMR Chemical Shift. *J. Am. Chem. Soc.* **2010**, *132*, 15505−15507.
(22) Berthault, P.; Desvaux, H.; Wendlinger, T.; Gyejacquot, M.; Stopin, A.; Brotin, T.; Dutasta, J. P.; Boulard, Y. Effect of pH and Counterions on the Encapsulation Properties of Xenon in Water-Soluble Cryptophanes. *Chem. - Eur. J.* **2010**, *16*, 12941−12946.
(23) Brotin, T.; Cavagnat, D.; Berthault, P.; Montserret, R.; Buffeteau, T. Water-Soluble Molecular Capsule for the Complexation of Cesium and Thallium Cations. *J. Phys. Chem. B* **2012**, *116*, 10905−10914.
(24) Brotin, T.; Montserret, R.; Bouchet, A.; Cavagnat, D.; Linares, M.; Buffeteau, T. High Affinity of Water-Soluble Cryptophanes for Cesium Cations. *J. Org. Chem.* **2012**, *77*, 1198−1201.
(25) Aski, S. N.; Lo, A. Y. H.; Brotin, T.; Dutasta, J. P.; Edén, M.; Kowalewski, J. Studies of Inclusion Complexes of Dichloromethane in Cryptophanes by Exchange Kinetics and C-13 NMR in Solution and the Solid State. *J. Phys. Chem. C* **2008**, *112*, 13873−13881.
(26) Takacs, Z.; Soltesova, M.; Kotsyubynskyy, D.; Kowalewski, J.; Lang, J.; Brotin, T.; Dutasta, J. P. NMR Investigation of Guest-Host Complex Between Chloroform and Cryptophane C. *Magn. Reson. Chem.* **2010**, *48*, 623−629.
(27) Takacs, Z.; Brotin, T.; Dutasta, J. P.; Lang, J.; Todde, G.; Kowalewski, J. Inclusion of Chloromethane Guests Affects Conformation and Internal Dynamics of Cryptophane-D Host. *J. Phys. Chem. B* **2012**, *116*, 7898−7913.
(28) Takacs, Z.; Soltesova, M.; Kowalewski, J.; Lang, J.; Brotin, T.; Dutasta, J. P. Host-Guest Complexes between Cryptophane-C and Chloromethanes Revisited. *Magn. Reson. Chem.* **2013**, *51*, 19−31.
(29) Takacs, Z.; Steiner, E.; Kowalewski, J.; Brotin, T. NMR Investigation of Chloromethane Complexes of Cryptophane-A and Its Analogue with Butoxy Groups. *J. Phys. Chem. B* **2014**, *118*, 2134−2146.
(30) Steiner, E.; Mathew, R.; Zimmermann, I.; Brotin, T.; Edén, M.; Kowalewski, J. Investigation of Chloromethane Complexes of Cryptophane-A Analogue with Butoxy Groups Using ^{13}C NMR in the Solid State and Solution along with Single Crystal X-ray Diffraction. *Magn. Reson. Chem.* **2015**, *53*, 596−602.
(31) Chaffee, K. E.; Fogarty, H. A.; Brotin, T.; Goodson, B. M.; Dutasta, J. P. Encapsulation of Small Gas Molecules by Cryptophane-111 in Organic Solution. 1. Size- and Shape-Selective Complexation of Simple Hydrocarbons. *J. Phys. Chem. A* **2009**, *113*, 13675−13684.
(32) Brotin, T.; Cavagnat, D.; Jeanneau, E.; Buffeteau, T. Synthesis of Highly Substituted Cryptophane Derivatives. *J. Org. Chem.* **2013**, *78*, 6143−6153.
(33) Taratula, O.; Hill, P. A.; Khan, N. S.; Carroll, P. J.; Dmochowski, I. J. Crystallographic Observation of 'Induced Fit' in a Cryptophane Host-Guest Model System. *Nat. Commun.* **2010**, *1*, 148.
(34) Woessner, D. E. Relaxation Effects of Chemical Exchange. In *Encyclopedia of Nuclear Magnetic Resonance*; Grant, D. M., Harris, R. K., Eds.; Wiley: Chichester, 1996; pp 4018−4028.
(35) Kowalewski, J.; Mäler, L. *Nuclear Spin Relaxation in Liquids*; Taylor and Francis: New York, 2006.
(36) Lipari, G.; Szabo, A. Model-Free Approach to the Interpretation of Nuclear Magnetic Resonance Relaxation in Macromolecules 1. Theory and Range of Validity. *J. Am. Chem. Soc.* **1982**, *104*, 4546−4559.
(37) Werbelow, L. G. Relaxation Processes: Cross Correlation and Interference Terms. In *Encyclopedia of Nuclear Magnetic Resonance*; Grant, D. M., Harris, R. K., Eds.; Wiley: Chichester, 1996; pp 4072−4078.
(38) Kumar, A.; Grace, R. C. R.; Madhu, P. K. Cross-Correlations in NMR. *Prog. Nucl. Magn. Reson. Spectrosc.* **2000**, *37*, 191−319.
(39) Shimizu, H. Theory of the Dependence of Nuclear Magnetic Relaxation on the Absolute Sign of Spin-Spin Coupling Constant. *J. Chem. Phys.* **1964**, *40*, 3357−3364.
(40) Goldman, M. Interference Effects in the Relaxation of a Pair of Unlike Spin-1/2 Nuclei. *J. Magn. Reson.* **1984**, *60*, 437−452.
(41) Werbelow, L. G.; Grant, D. M. Intramolecular Dipolar Relaxation in Multispin Systems. *Adv. Magn. Reson.* **1977**, *9*, 189−299.
(42) Canet, D. Relaxation Mechanisms: Magnetization Modes. In *Encyclopedia of Nuclear Magnetic Resonance*; Grant, D. M., Harris, K. R., Eds.; Wiley: Chichester, 1996; pp 4046−4053.
(43) Kloiber, K.; Konrat, R. Differential Multiple-Quantum Relaxation Arising from Cross-Correlated Time Modulation of Isotropic Chemical Shifts. *J. Biomol. NMR* **2000**, *18*, 33−42.
(44) Früh, D.; Tolman, J. R.; Bodenhausen, G.; Zwahlen, C. Cross-Correlated Chemical Shift Modulation: A Signature of Slow Internal Motions in Proteins. *J. Am. Chem. Soc.* **2001**, *123*, 4810−4816.
(45) Lundström, P.; Akke, M. Quantitative Analysis of Conformational Exchange Contributions to H-1-N-15 Multiple-Quantum Relaxation Using Field-Dependent Measurements. Time Scale and Structural Characterization of Exchange in a Calmodulin C- Terminal Domain Mutant. *J. Am. Chem. Soc.* **2004**, *126*, 928−935.
(46) Kroenke, C. D.; Loria, J. P.; Lee, L. K.; Rance, M.; Palmer, A. G. Longitudinal and Transverse H-1-N-15 Dipolar N-15 Chemical Shift Anisotropy Relaxation Interference: Unambiguous Determination of Rotational Diffusion Tensors and Chemical Exchange Effects in Biological Macromolecules. *J. Am. Chem. Soc.* **1998**, *120*, 7905−7915.
(47) Peng, J. W. Cross-Correlated F-19 Relaxation Measurements for the Study of Fluorinated Ligand-Receptor Interactions. *J. Magn. Reson.* **2001**, *153*, 32−47.
(48) Peng, J. W. New Probes of Ligand Flexibility in Drug Design: Transferred C-13 CSA- Dipolar Cross-Correlated Relaxation at Natural Abundance. *J. Am. Chem. Soc.* **2003**, *125*, 11116−11130.

DOI: 10.1021/acs.jpcb.5b05218
J. Phys. Chem. B 2015, 119, 11760−11767

(49) Skrynnikov, N. R.; Ernst, R. R. Detection of Intermolecular Chemical Exchange through Decorrelation of Two-Spin Order. *J. Magn. Reson.* **1999**, *137*, 276−280.
(50) Esadze, A.; Li, D. W.; Wang, T. Z.; Brüschweiler, R.; Iwahara, J. Dynamics of Lysine Side-Chain Amino Groups in a Protein Studied by Heteronuclear H-1-N-15 NMR Spectroscopy. *J. Am. Chem. Soc.* **2011**, *133*, 909−919.
(51) Werbeck, N. D.; Hansen, D. F. Heteronuclear Transverse and Longitudinal Relaxation in AX_4 Spin Systems: Application to ^{15}N relaxations in $^{15}NH_4$+. *J. Magn. Reson.* **2014**, *246*, 136−148.
(52) Bodenhausen, G.; Wagner, G.; Rance, M.; Sorensen, O. W.; Wüthrich, K.; Ernst, R. R. Longitudinal 2-Spin Order in 2D Exchange Spectroscopy (NOESY). *J. Magn. Reson.* **1984**, *59*, 542−550.
(53) Wagner, G.; Bodenhausen, G.; Müller, N.; Rance, M.; Sorensen, O. W.; Ernst, R. R.; Wüthrich, K. Exchange of Two-Spin Order in Nuclear Magnetic Resonance: Separation of Exchange and Cross-Relaxation Processes. *J. Am. Chem. Soc.* **1985**, *107*, 6440−6446.
(54) Jaccard, G.; Wimperis, S.; Bodenhausen, G. Observation of 2IzSz Order in NMR Relaxation Studies for Measuring Cross-Correlation of Chemical Shift Anisotropy and Dipolar Interactions. *Chem. Phys. Lett.* **1987**, *138*, 601−606.
(55) Boyd, J.; Hommel, U.; Campbell, I. D. Influence of Cross-Correlation Between Dipolar and Anisotropic Chemical Shift Relaxation Mechanisms upon Longitudinal Relaxation Rates of N-15 in Macromolecules. *Chem. Phys. Lett.* **1990**, *175*, 477−482.
(56) Redfield, A. G. The Theory of Relaxation Processes. *Adv. Magn. Reson.* **1965**, *1*, 1−32.
(57) Abragam, A. *The Principles of Nuclear Magnetism*; Oxford University Press: Oxford, 1961.
(58) Ernst, R. R.; Bodenhausen, G.; Wokaun, A. *Principles of Nuclear Magnetic Resonance in One and Two Dimensions*; Clarendon Press: Oxford, 1987.
(59) Helgstrand, M.; Härd, T.; Allard, P. Simulations of NMR Pulse Sequences during Equilibrium and Non-Equlibrium Chemical Exchange. *J. Biomol. NMR* **2000**, *18*, 49−63.
(60) Auer, R.; Tollinger, M.; Kuprov, I.; Konrat, R.; Kloiber, K. Mathematical Treatment of Adiabatic Fast Passage Pulses for the Computation of Nuclear Spin Relaxation Rates in Proteins with Conformational Exchange. *J. Biomol. NMR* **2011**, *51*, 35−47.
(61) Bhattacharyya, R.; Kumar, A. Use of Cross-Correlated NMR Relaxation for the Study of Motional Anisotropy of Liquid Crystals. *Chem. Phys. Lett.* **2003**, *372*, 35−44.
(62) Ernst, M.; Ernst, R. R. Heteronuclear Dipolar Cross-Correlated Cross Relaxation for the Investigation of Side-Chain Motions. *J. Magn. Reson., Ser. A* **1994**, *110*, 202−213.
(63) Hanselman, D. C.; Littlefield, B. R. *Mastering Matlab 6: A Comprehensive Tutorial and Reference*; Prentice Hall: Upper Saddle River, NJ, 2001.
(64) Lang, J.; Dechter, J. J.; Effemey, M.; Kowalewski, J. Dynamics of an Inclusion Complex of Chloroform and Cryptophane-E: Evidence for a Strongly Anisotropic van der Waals Bond. *J. Am. Chem. Soc.* **2001**, *123*, 7852−7858.
(65) Ghosh, S. N.; Trambarulo, R.; Gordy, W. Microwave Spectra and Molecular Structures of Fluoroform, Chloroform, and Methyl Chloroform. *J. Chem. Phys.* **1952**, *20*, 605−607.
(66) Mäler, L.; Kowalewski, J. Cross-Correlation Effects in the Longitudinal Relaxation of Heteronuclear Spin Systems. *Chem. Phys. Lett.* **1992**, *192*, 595−600.
(67) Bhattacharyya, P. K.; Dailey, B. P. 13C and 1H Chemical-Shift Anisotropies in Chloroform. *J. Magn. Reson.* **1973**, *12*, 36−39.
(68) Hiltunen, Y. Determination of the C-13 Shielding Tensors for Methyl Halides and Haloforms by NMR in Mixtures of Liquid-Crystals. *Mol. Phys.* **1987**, *62*, 1187−1194.
(69) Vaara, J.; Oikarinen, K.; Jokisaari, J.; Lounila, J. Anisotropy of the H-1 and C-13 Shielding Tensors in Chloroform. *Chem. Phys. Lett.* **1996**, *253*, 340−348.
(70) Vaara, J.; Lounila, J.; Jokisaari, J. Comment on "Nematic Mixture Methods for the Determination of Chemical Shift Anisotropy". *Chem. Phys. Lett.* **1998**, *296*, 541−544.
(71) Marjanska, M.; Goodson, B. M.; Castiglione, F.; Pines, A. Inclusion Complexes Oriented in Thermotropic Liquid-Crystalline Solvents Studied with Carbon-13 NMR. *J. Phys. Chem. B* **2003**, *107*, 12558−12561.
(72) Chaffee, K. E.; Marjanska, M.; Goodson, B. M. NMR Studies of Chloroform@Cryptophane-A and Chloroform@Bis-Cryptophane Inclusion Complexes Oriented in Thermotropic Liquid Crystals. *Solid State Nucl. Magn. Reson.* **2006**, *29*, 104−112.

DOI: 10.1021/acs.jpcb.5b05218
J. Phys. Chem. B 2015, 119, 11760−11767